# On the Relation between the Hydrated Electron Solvation Structure and Its Partial Molar Volume

Pauf Neupane,<sup>†</sup> David M. Bartels,\*,<sup>‡</sup> and Ward H. Thompson\*,<sup>†</sup>

†Department of Chemistry, University of Kansas, Lawrence, KS 66045, USA ‡Radiation Laboratory, University of Notre Dame, Notre Dame, Indiana 46556, United States

E-mail: bartels.5@nd.edu; wthompson@ku.edu

July 26, 2023

#### Abstract

It is now generally accepted that the hydrated electron occupies a cavity in water, but the size of the cavity and the arrangements of the solvating water molecules are not fully characterized. Here, we use the Kirkwood-Buff (KB) approach to examine how the partial molar volume  $(V_M)$  provides insight into these issues. The KB method relates  $V_M$  to an integral of the electron-water radial distribution function, a key measure of the hydrated electron structure. We have applied it to three widely-used pseudopotentials and the results show that  $V_M$ is a sensitive measure of the fidelity of hydrated electron descriptions. Thus, the measured  $V_M$  places constraints on the hydrated electron structure that are important in developing and evaluating model descriptions. Importantly, we find that  $V_M$  does not reflect only the cavity size (and thus should not be used to infer the cavity radius), but is strongly dependent on the extended solvation structure.

## 1 Introduction

The hydrated electron has attracted significant theoretical and experimental attention, particularly over the past three decades. A key focus of investigations has been the accurate characterization of its structure. One aspect of this is whether the electron resides in a cavity or, alternatively, adopts a non-cavity structure in which it densifies the water molecules in its vicinity. <sup>1–4</sup> This argument has now been settled in favor of a cavity picture, <sup>4–7</sup> but the details of the structure still require elucidation, including the size of the cavity and the arrangements of the solvating water molecules.

One reason that the picture of the hydrated electron structure remains unsettled is the challenge in modeling it. Two primary approaches have been used that each have advantages and limitations. Many of the earliest efforts, which continue to the present, used mixed quantumclassical molecular dynamics (QC-MD) simulations in which the quantum electron interacts with classical water molecules through an effective one-electron pseudopotential.<sup>8,9</sup> Typically the electron is described adiabatically by solving its Schrödinger equation at every step in the classical simulation of the water molecules. This enables relatively long simulation times and large system sizes, but has the drawback that the quality of the results depends on the accuracy of the pseudopotential (and the oneelectron approximation). Several pseudopotentials have been developed, 1,9-12 but so far none appear capable of adequately reproducing all of the experimentally measured characteristics of the hydrated electron.

More recently, with the development of improved codes and the increase in computer speeds, *ab initio* molecular dynamics (AIMD) simulations have become more prevalent. <sup>3,6,13–20</sup> They are, however, limited by the computational effort required. Indeed, Park and Schwartz recently carried out an analysis that indicated such simulations are not converged at the currently feasible system sizes. <sup>6</sup> This fact also makes it more difficult to analyze the accuracy of different functionals. On the other hand, AIMD simulations are not limited by the one-electron approximation and certainly provide a more accurate representation of the hydrated electron than currently available pseudopotentials.

These challenges for both pseudopotential and AIMD simulation approaches have motivated a strong focus on testing how well different computational descriptions are able to reproduce experimental characterizations. 2,4,6,21 Chief among these are the vertical detachment energy<sup>22–24</sup> and radius of gyration.<sup>2,25–27</sup> These properties probe the strength of the electron binding as well as the degree of delocalization of its wavefunction. They are, however, not sufficient to constrain the pseudopotential description; both the Turi-Borgis<sup>10</sup> (TB) and optimized Turi-Borgis<sup>12</sup> pseudopotentials adequately describe the hydrated electron radius of gyration and vertical detachment energy, but are inaccurate in predictions of other hydrated electron properties.<sup>2,12</sup> On the other hand, AIMD efforts often give smaller values for both quantities compared to experiment, 3,6,19,28,29 likely due primarily to the small system sizes. 6

A key property that deserves greater attention is the partial molar volume,  $V_M$ , which measures the change in volume of the solution upon addition of hydrated electrons. Like the radius of gyration and vertical detachment energy, it has been accurately determined experimentally as  $V_M = 26 \pm 6 \text{ cm}^3/\text{mol},^{7,30}$  i.e., the solution expands when a hydrated electron is added. However, it has, to our knowledge, only been calculated by Schwartz and coworkers, 12,31 who used an approach in which they calculated the volume of a water slab in a vacuum with and without a hydrated electron present. As we demonstrate here, there is

much more to be learned from calculating the partial molar volume than just its value for a given model.

In this Paper, we apply the approach for calculating the partial molar volume developed by Kirkwood and Buff to the hydrated electron. To our knowledge, this is the first application of this method to a solvated electron system. It has a number of advantages that we exploit here. It provides a rigorous framework for computing the partial molar volume that can be systematically converged with respect to system size and statistical sampling. Further, because it gives the partial molar volume in terms of the electron-water radial distribution function (RDF), it provides a direct relationship to the hydrated electron structure. This has multiple implications. On the one hand, we can use the measured partial molar volume, in the context of simulation results, to draw inferences about the properties of the actual electron-water radial distribution function. On the other hand, we can use the calculations to determine the contributions to  $V_M$  due to the different regions of the RDF, e.g., the cavity and the first few water solvation shells, as has been done for other solutes previously. 32,33 Such analyses challenge the traditional interpretation of the partial molar volume as a measure of the cavity size $^{4,34,35}$  (vide infra).

# 2 Methods

# 2.1 Theory

Kirkwood and Buff showed that, in the infinite dilution limit, thermodynamical quantities such as compressibility and partial molar volume can be expressed in terms of integrals of the radial distribution function. <sup>36,37</sup> In particular, the Kirkwood-Buff (KB) integral for an open system is written as

$$G_{\alpha\beta} = \int_0^\infty [g_{\alpha\beta}(r) - 1] 4\pi r^2 dr, \qquad (1)$$

where  $g_{\alpha\beta}(r)$  is the RDF for the centers-of-mass of solute  $\alpha$  and solvent  $\beta$  as a function of the distance r, and the integration extends through an infinitely large volume. Then, the partial molar volume can be computed from the KB integral as  $^{37}$ 

$$V_M = k_B T \kappa_T - G_{\alpha\beta},\tag{2}$$

where  $k_B$  is the Boltzmann constant, T is the absolute temperature, and  $\kappa_T$  is the isothermal compressibility of the solvent. Here, we take  $\kappa_T = 4.50 \times 10^{-5} \text{ atm}^{-1}$ , which is obtained from the water model used in the simulations, <sup>38</sup> such that  $k_B T \kappa_T = 1.10 \text{ cm}^3/\text{mol}$ .

In principle, the KB integral,  $G_{\alpha\beta}$ , should be obtained from an infinite, open system. In practice, one approximates it based on simulations of finite, closed systems. In this case, it can be important to modify Eq. 1 to account for the finite size of the simulation system as, <sup>39–42</sup>

$$G_{\alpha\beta} = \int_0^R [g_{\alpha\beta}(r) - 1] w(r; R) dr, \qquad (3)$$

where R is the maximum r for which the RDF is available. Here, R is taken to be the distance of the last histogram bin used in computing  $g_{\alpha\beta}(r)$  and thus,  $R \simeq L/2$ , where L is the side length of the cubic simulation cell. The w(r;R) is a weighting function, for which Krüger and Vlugt derived an analytical expression,  $^{40-42}$ 

$$w(r;R) = 4\pi r^2 \left(1 - \frac{3x}{2} + \frac{x^3}{2}\right),$$
 (4)

where x = r/R.

# 3 Computational Methods

# 3.1 One-Electron Pseudopotentials

In this work, we utilize the electron-water RDF obtained from QC-MD simulations and the KB integral to compute the partial molar volume of the hydrated electron using Eqs. 3 and 4. A full description is provided in the Computational Details, but briefly, the water molecules are described classically, with the fixed-charge, flexible SPC/Fw force field, <sup>38</sup> while the electron is described quantum mechanically within an adi-

abatic approximation. The electron interacts with the water molecules through a pseudopotential. In this work, we consider three pseudopotentials that have been introduced in the literature for describing the hydrated electron: Turi-Borgis (TB), <sup>10</sup> the optimized Turi-Borgis (TBOpt, also known as TBSE+OptPol), <sup>12</sup> and Larsen-Glover-Schwartz (LGS). <sup>1</sup> All three pseudopotentials were developed based on the static-exchange (SE) approximation for the excess electron wave function.

The TB pseudopotential describes the hydrated electron as residing in a cavity and primarily interacting with the first solvation shell of water molecules. This model appears to give electron structures that are too rigid compared to experimental characterizations and *ab initio* descriptions. To address this, Glover and Schwartz<sup>12</sup> proposed the TBOpt pseudopotential, which differs in the polarization potential. Both the TB and TBOpt pseudopotentials use a simple functional form for the excess electron interaction potential with oxygen (ox) and hydrogen (hy) sites,

$$V_{x}(r_{x}) = -\frac{q_{x}}{r_{x}} \operatorname{erf}(A_{1,x}r_{x})$$

$$+ \frac{B_{1,x}}{r_{x}} \left[ \operatorname{erf}(B_{2,x}r_{x}) - \operatorname{erf}(B_{3,x}r_{x}) \right],$$
(5)

where x refers to ox or hy and  $r_x$  is the electronx site distance. This potential has eight parameters  $(A_{1,x}, B_{i,x})$  whose values are listed in Ref. 10 and  $q_x$  are the water site charges (-0.82e for oxygen and 0.41e for hydrogen in the SPC/Fw model). The full pseudopotential also includes a polarization potential, which is added a posteriori as,

$$V_{pol} = -\frac{\alpha}{2(r_{ox}^2 + C_{1,ox}^2)^2}. (6)$$

The TB pseudopotential assumes  $\alpha$  to be the polarizability of the water molecule ( $\alpha = 9.7446$  a.u.), and the parameter  $C_{1,ox} = 4.4$  a.u. is adjusted to reproduce the ground state energy of the hydrated electron. <sup>10</sup> The TBOpt model was obtained by changing only the polarization potential such that  $\alpha = 9.25$  a.u. and  $C_{1,ox} = 2.07$  a.u., to better match the coupled-

cluster singles and doubles with perturbative triples (CCSD(T)) interaction energies.<sup>12</sup>

The LGS pseudopotential is known to generate a non-cavity description of the hydrated electron, *i.e.*, it does not exclude water molecules from the region where the electron resides. The functional form of this pseudopotential is

$$V(\mathbf{r}) = \sum_{n=1}^{8} B_n |\mathbf{r} - \mathbf{r}_n|^{i_n} e^{-\rho_n |\mathbf{r} - \mathbf{r}_n|^2} + V_C(\mathbf{r}), (7)$$

where n labels functions for which  $r_n$  represents the locations of the oxygen or hydrogen water sites;  $V_C$  is the total Coulombic interaction (electron-oxygen and electron-hydrogen) taken to be  $-q/r_x$  for  $r_x \geq r_{cut}$  and  $-q\left(\frac{3}{2r_{cut}} - \frac{r_x^2}{2r_{cut}^3}\right)$  for  $r_x < r_{cut}$ . Then the polarization potential is added as

$$V_{pol} = -\frac{\alpha}{2r_{ox}^4} \left[ 1 - e^{-(r_{ox}/r_c)^6} \right], \tag{8}$$

where  $\alpha = 9.745$  a.u. is the water polarizability and  $r_c = 1.53$  Å.

We note that the large system size and extensive statistical sampling required to calculate the KB integral is enabled by these one-electron pseudopotential approaches.

#### 3.2 Simulation Details

All simulations were performed using our inhouse QC-MD simulation code. Initially, a cubic water box of 2048 molecules and side length 39.462319 Å is relaxed using classical MD in the microcanonical (NVE) ensemble for 50 ps. followed by further equilibration of 250 ps in an isothermal-isobaric (NPT) ensemble. Then an electron is introduced, and an NPT simulation is performed for 13 ps in the mixed quantum classical regime, of which the last 10 ps is used for data analysis. We have propagated 3 sets of 60 such trajectories for TB, yielding a total of 1.8 ns for data analysis. Similarly, for TBOpt and LGS models, we propagated 3 sets of 40 and 20 trajectories, respectively. The simulations with LGS are more expensive as this model requires a more denser basis to evaluate the electron wavefunction.

We have used periodic boundaries in all directions throughout the simulations. Initial velocities are assigned randomly at 298.15 K, drawn from the Boltzmann distribution. The classical equations of motion are integrated with the velocity Verlet algorithm using a time step of 1 fs. Temperature is maintained at 298.15 K using a Bussi-Donadio-Parrinello thermostat. 43 The Bernetti-Bussi barostat is used to maintain a pressure of 1 atm in the NPT simulations, ensuring sampling in the isothermal-isobaric ensemble. 44 The Lennard-Jones interactions are truncated at 19 Å, which is approximately half of the simulation cell dimension. The solventsolvent long-range electrostatic interactions are handled using the Ewald sum method, with the real space part truncated at 19 Å. 45,46 As is discussed in the Supporting Information, this size of the simulation cell and cutoff radius are sufficient to accurately converge the partial molar volume. We also present results for the partial molar volume of Br<sup>-</sup> in the Supporting Information with and without the presence of a Na<sup>+</sup> counterion to illustrate the use of a charge simulation cell does not affect the results.

For the quantum mechanical calculation of the adiabatic electron wavefunction at each time step in the QC-MD simulation, the Schrödinger equation is solved using a sincfunction discrete variable representation (DVR) basis. <sup>47</sup> The DVR basis spans from -7 to 6.125 Å with  $16 \times 16 \times 16$  grids (grid spacing 0.875 Å) for the TB and TBOpt models, and  $32 \times 32 \times 32$  grids (grid spacing 0.4375 Å) for the LGS pseudopotential. The eigenvalue equation is solved using an iterative Lanczos algorithm with full reorthogonalization.

All error bars are reported as 95% confidence intervals based on the Student's t-distribution <sup>48</sup> using block averaging with 3 blocks, each consisting of 20, 40, or 60 ten-picosecond trajectories for the LGS, TBOpt, and TB models, respectively, as described above.

## 4 Results and Discussion

We have calculated the RDF between the hydrated electron and water molecule center-of-

mass for each of the three pseudopotentials using the approach detailed above. These results are shown in Fig. 1, with shaded regions representing the error bars. The RDFs are consistent with those reported in previous studies for  $e^-$ -oxygen,  $^{1,12,49}$  typically with less statistical sampling. Note that most simulations of the hydrated electron with one-electron pseudopotentials have used the SPC/Flexible water model,  $^{50}$  which has the same site charges but a more complex intramolecular potential. We previously found that the two water models yield similar behavior for the TB and LGS models.  $^{49}$ 

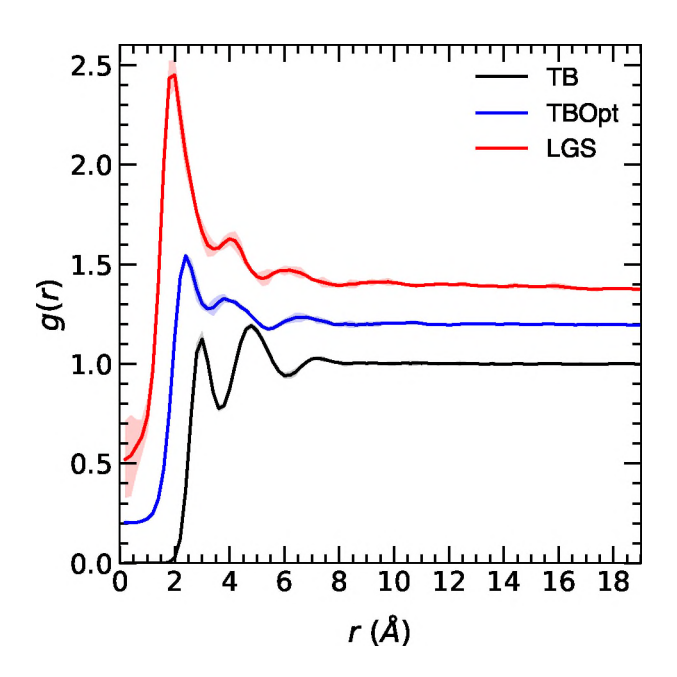


Figure 1: The  $e^-$ -water radial distribution function, g(r), for the TB (black), TBOpt (blue), and LGS (red) pseudopotential hydrated electrons. The RDFs for the TBOpt and LGS are shifted upward by 0.2 and 0.4, respectively, for clarity. The shaded regions show error bars as 95% confidence limits.

The RDFs illustrate the clear differences between the three pseudopotentials that have important implications for the hydrated electron partial molar volume (vide infra). The nature of the electron cavity is the first of these. The TB model completely excludes water molecules from a 2 Å radius around the center-of-mass of the hydrated electron. In contrast, the non-cavity nature of the LGS pseudopotential

is evident in the non-zero  $e^-$ -water RDF for all distances, including as r approaches zero. As noted previously, the LGS electron fluctuates between cavity and non-cavity structures, presenting non-cavity behavior overall. <sup>5,49</sup> The TBOpt model yields an RDF that lies in between these two. The RDF is zero (within error bars) only for r < 0.75 Å and begins to rise sharply around 1-1.5 Å. Thus, it exhibits a smaller, weaker cavity, as intended in its design. <sup>12</sup>

A second key difference between the RDFs of the three models is the solvation structure. The TB model has a weakly structured first solvation shell as measured by the height of the first peak (1.12 at 3.0 Å) which is even smaller than the second solvation shell peak (1.19 at 4.8 Å). In between the first and second, as well as second and third, solvation shells the RDF falls below one. These behaviors are in sharp contrast with the LGS pseudopotential. It has a large, sharp peak (2.05 at 2.0 Å) associated with the first solvation shell with a dramatically smaller second solvation shell peak (1.23 at 4.0 Å) and the RDF remains at or above one between the first three solvation shells. Once again, the TBOpt model gives an intermediate description of the hydrated electron. Like the LGS model, it has a comparatively large first solvation shell peak (1.34 at 2.4 Å) and a smaller second solvation shell (1.13 at 3.8 Å), but these occur with smaller magnitudes than for the LGS case. The RDF does not fall below one between these two peaks, but does between the second and third solvation shells.

These RDFs are used to compute the KB integrals (Eq. 3) and the partial molar volume (Eq. 2) of the hydrated electron. The running integrals used to compute the partial molar volume are shown in Fig. 2 and compared to the experimental result. It is useful to first note the effect of the RDF features on the partial molar volume. The excluded volume associated with a hydrated electron cavity appears as positive contribution to the partial molar volume, *i.e.*, volume needed in the solution to accommodate the electron. Note that for all three pseudopotentials, this appears as a rise in the partial molar volume integral at small r, which is

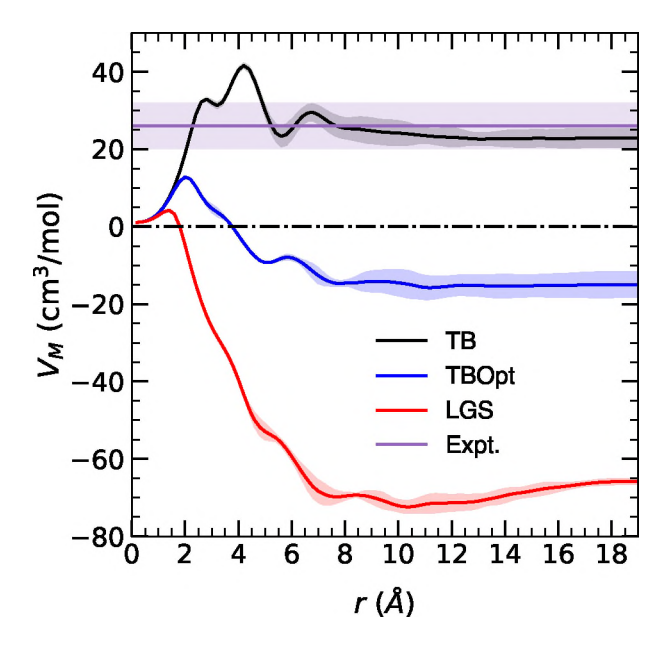


Figure 2: Partial molar volumes for TB (black), TBOpt (blue), and LGS (red) hydrated electrons shown as the running integral in Eq. 2. The experimental value (violet) is also shown for comparison. The shaded regions show error bars as 95% confidence limits.

largest for the TB model but quite small for the non-cavity LGS model. At larger distances, the structure of the solvation shells strongly modifies  $V_M$ . Namely, larger peaks correspond to greater water densification induced around the hydrated electron and lead to a decrease in the partial molar volume. Regions of the RDF between solvation shells that fall below one have the opposite effect, increasing  $V_M$ . Note that the  $4\pi r^2$  factor in the integral, Eq. 3, plays an important role as it amplifies the behavior of the RDF to account for the larger number of water molecules present as r increases.

Both the comparatively large, rigid cavity and the modest solvation shell structure predicted by the TB pseudopotential tend to increase the partial molar volume. Our calculated result is  $V_M = 23 \pm 3$  cm<sup>3</sup>/mol, which is unambiguously positive and also in quantitative agreement with the measured value of  $26\pm 6$  cm<sup>3</sup>/mol obtained by Janik et al.<sup>7</sup> and Borsarelli et al.<sup>30</sup> The present result is also in accord with that previously estimated by Casey et al. for the TB model as  $31 \pm 12$  cm<sup>3</sup>/mol.<sup>31</sup> They used a quite different approach in which they carried

out simulations of water in a slab geometry with two air-water interfaces. They used a grid to estimate the location of the surface atoms and thereby compute the volume of the water slab with and without the hydrated electron present.

Note that the Kirkwood-Buff approach provides insight into the origin of the partial molar volume value. In particular, by considering the contributions to  $V_M$  from different regions of the RDF, we can determine the influence of each part of the hydrated electron structure on the partial molar volume. These results are presented in Fig. 3 and obtained as follows. We can view the cavity contribution as that associated with the KB integral up to the distance where the RDF first rises to one, around r = 2.7 Åfor the TB model; at this point the TB partial molar volume is approximately 33 cm<sup>3</sup>/mol. The contributions of the water solvation shells are similarly estimated from the net contribution to the KB integral over the distances of each shell. We use the minima between the solvation shell peaks as dividing points and the point where the RDF first reaches one as the beginning of the first solvation shell as illustrated in Fig. 3a. Again considering the TB case, this shows a small positive contribution of  $\sim 2 \text{ cm}^3/\text{mol to } V_M$  from the first solvation shell, as can be seen in Fig. 3b; the fact that this component is positive can be attributed to the reduced water density between the first and second solvation shells. However, the larger second solvation shell peak leads to a significant negative contribution of  $-9 \text{ cm}^3/\text{mol}$ . The third solvation shell has little contribution to the partial molar volume. Note that these results illustrate that the partial molar volume cannot be considered to come solely from the cavity, even for this pseudopotential that yields the most rigid cavity behavior. Conversely, this indicates that the partial molar volume should not be used to infer the cavity size.

The non-cavity LGS pseudopotential gives a large, negative partial molar volume of  $V_M = -66 \text{ cm}^3/\text{mol}$ . The small positive contribution to  $V_M$  of 4 cm<sup>3</sup>/mol from the limited exclusion of water molecules around the center of the electron distribution, the "cavity," is more than cancelled by the strong water structuring

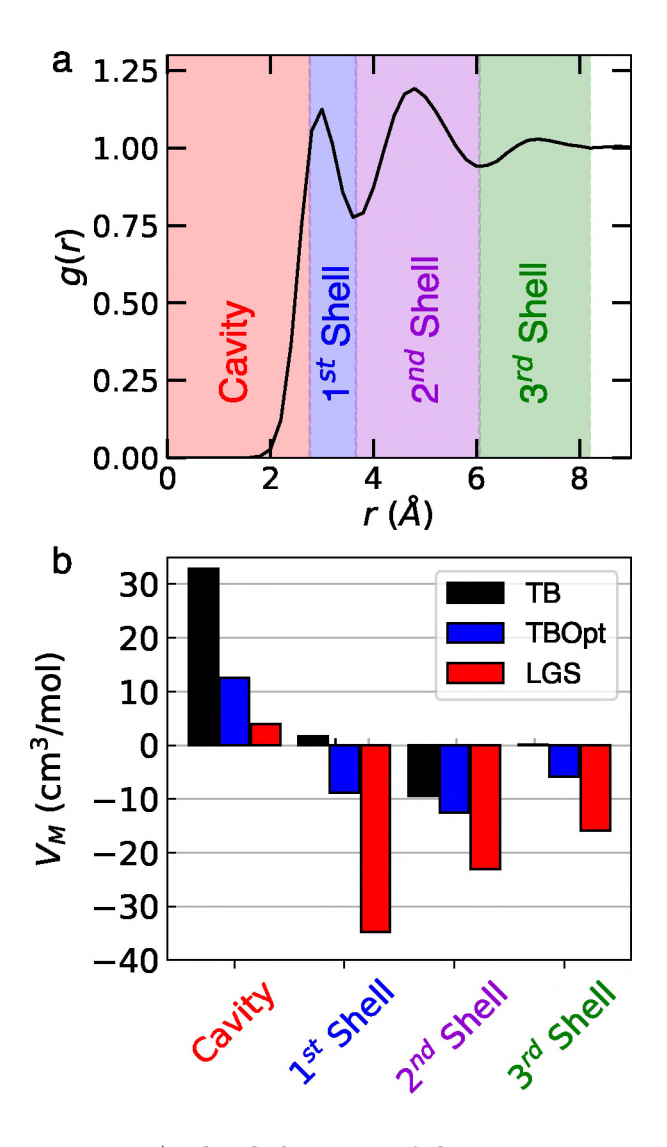


Figure 3: a) The definitions of the cavity region as well as the first, second, and third water solvation shells are illustrated for the TB model; see the text for further details. b) The estimated contributions to the partial molar volume from each region are shown for the TB (black), TBOpt (blue), and LGS (red) pseudopotentials.

in the solvation shells. As shown in Fig. 3, the first solvation shell reduces the partial molar volume by  $\sim 35 \text{ cm}^3/\text{mol}$ , the second solvation shell by another 23 cm<sup>3</sup>/mol, and the third by another 16 cm<sup>3</sup>/mol. As can be seen from Fig. 2, the running integral for  $V_M$  reaches a plateau around  $-71 \text{ cm}^3/\text{mol}$  before rising to the final value we reported above. This rise is associated with a diminished density we find at larger distances from the electron (see Fig. 1) that is likely associated with the finite simulation box and the strongly attractive nature of the LGS hydrated electron; we do not see such behavior for the less attractive TB and TBOpt pseudopotentials. Accounting for this, our best estimate of the LGS partial molar volume is  $V_M = -68 \pm 5 \text{ cm}^3/\text{mol}$ . This is smaller in magnitude than the value of  $-116\pm17$  cm<sup>3</sup>/mol obtained by Casev et al. 31

Finally, we consider the results for the TBOpt pseudopotential. As expected, they are intermediate between the cavity-forming TB and non-cavity LGS models. Importantly, however, the partial molar volume we obtain for the TBOpt model is  $V_M = -15 \pm 4 \text{ cm}^3/\text{mol}$ , which is at odds with the positive measured value, <sup>7,30</sup> but agrees with the  $-14 \pm 12$  cm<sup>3</sup>/mol reported by Glover and Schwartz<sup>12</sup> using the approach of Ref. 31. The negative  $V_M$  can be understood in terms of the changes to the cavity and solvation structure relative to the TB pseudopotential from which it was derived. First, the contribution of the cavity to the partial molar volume, shown in Fig. 3, is  $\sim 12.5 \text{ cm}^3/\text{mol}$ , a little more than a third of the TB result. The greater difference comes from the solvation structure, which more closely resembles the LGS behavior than that of the TB model. It leads to decreases in  $V_M$  of 9, 13, and 6 cm<sup>3</sup>/mol due to the first, second, and third solvation shells, respectively. These are individually of the same magnitude (though opposite sign) from the cavity contribution and taken together demonstrate a much stronger influence for the solvation structure than the cavity volume. The present results show that, while the TBOpt pseudopotential improves on a number of features of the TB model, it is not accurately describing the solvation of the hydrated electron as measured

by the partial molar volume. Moreover, the results implicate the solvation structure produced by the TBOpt pseudopotential as the origin of the deviation in  $V_M$  relative to experiment.

It is interesting to consider the RDFs obtained from ab initio MD (AIMD) in the context of these results. Park and Schwartz have recently demonstrated that, to this point, the published AIMD results are not converged with respect to system size, 6 which also limits the ability to calculate the KB integral to obtain the partial molar volume. While this is true, we can use published results to estimate some of the contributions to  $V_M$ . In general, the AIMD results do show a relatively consistent picture of the RDF with a smaller cavity than the TB model but stronger solvation shell structure: The peak maxima rise to 1.7 - 2.5 and the minima dip to 0.25 - 0.7.  $^{3,6,17,19,35}$  (This strong solvent structuring is similar to that observed for the bromide ion results shown in the Supporting Information.) We can use the KB integral with the largest system size (128 water molecules) RDF obtained by Park and Schwartz<sup>6</sup> to estimate the cavity as well as first and second solvation shell contributions to the partial molar volume, with the additional caveat that the simulations are at constant volume rather than constant pressure. We find the cavity contribution is  $\sim 9 \text{ cm}^3/\text{mol}$ , while the first solvation shell decreases  $V_M$  by roughly 6 cm<sup>3</sup>/mol and the second increases it by  $\sim 3 \text{ cm}^3/\text{mol}$ . While the net effect of these three contributions is positive, as seen above, the third solvation shell and beyond can have significant effects on the partial molar volume, which prevents the determination of  $V_M$  from these smaller AIMD simulations. However, it is interesting to note that the second solvation shell contribution is at odds with all three pseudopotential models, while the first solvation shell result is only in accord with that of the TBOpt model (albeit for quite different reasons given the divergent shapes of the RDFs).

#### 5 Conclusions

We have presented calculations of the partial molar volume of the hydrated electron within three different one-electron psuedopotential descriptions. The results show that the partial molar volume is a quite sensitive property for evaluating models. We find that only the TB model agrees with the measured partial molar volume, while both the TBOpt and LGS models yield values that have the opposite sign, consistent with prior calculations. <sup>12,31</sup>

A key focus of the present work is to exploit the Kirkwood-Buff approach to elucidate the origin of the sensitivity of the partial molar volume to the hydrated electron description. In particular, it shows the features the electron-water radial distribution function must have to reproduce the correct partial molar volume. While the presence of a cavity is a key aspect of this, a previously overlooked factor is the role of the water solvation structure, extending out multiple solvation shells. Importantly, these effects mean that  $V_M$  should not be used to estimate the hydrated electron cavity size. 4,34,35 Of the three models considered here, the TB pseudopotential provides a description that is in greatest accord with the measured  $V_M$ . However, the TB pseudopotential is known to have some important shortcomings, that the TBOpt description was developed to address. 12 and both are at odds with the RDFs obtained from AIMD simulations. Thus, the present results indicate there is additional progress to be made in developing a pseudopotential that provides an accurate, holistic description that includes reproducing the partial molar volume and, conversely, that the partial molar volume should be considered as a key metric in the assessment of such models.

# **Supporting Information**

Effects of simulation cell size and inclusion of counterions on the calculation of partial molar volumes

# Acknowledgments

This work was funded by the Division of Chemical Sciences, Geosciences, and Biosciences, Office of Basic Energy Sciences of the U.S. Department of Energy, through Grant No. DESC0021114 (W.H.T.). D.M.B. is supported by the U.S. Department of Energy Office of Science, Office of Basic Energy Sciences under Award Number DE-FC02-04ER1553. The calculations were performed at the University of Kansas Center for Research Computing (CRC), including including the BigJay cluster resource funded through NSF Grant MRI-2117449.

#### References

- (1) Larsen, R. E.; Glover, W. J.; Schwartz, B. J. Does the hydrated electron occupy a cavity? *Science* **2010**, 329, 65–69.
- (2) Turi, L.; Rossky, P. J. Theoretical studies of spectroscopy and dynamics of hydrated electrons. *Chem. Rev.* **2012**, *112*, 5641–5674.
- (3) Uhlig, F.; Marsalek, O.; Jungwirth, P. Unraveling the complex nature of the hydrated electron. J. Phys. Chem. Lett. **2012**, 3, 3071–3075.
- (4) Herbert, J. M. Structure of the aqueous electron. *Phys. Chem. Chem. Phys.* **2019**, 21, 20538–20565.
- (5) Glover, W. J.; Schwartz, B. J. The fluxional nature of the hydrated electron: Energy and entropy contributions to aqueous electron free energies. *J. Chem. Theory Comput.* **2020**, *16*, 1263–1270.
- (6) Park, S. J.; Schwartz, B. J. Understanding the temperature dependence and finite size effects in *ab initio* MD simulations of the hydrated electron. *J. Chem. Theory Comput.* **2022**, *18*, 4973–4982.
- (7) Janik, I.; Lisovskaya, A.; Bartels, D. M. Partial molar volume of the hydrated elec-

- tron. J. Phys. Chem. Lett. **2019**, 10, 2220–2226.
- (8) Schnitker, J.; Rossky, P. J. Quantum simulation study of the hydrated electron. *J. Chem. Phys.* **1987**, *86*, 3471–3485.
- (9) Schnitker, J.; Rossky, P. J. An electronwater pseudopotential for condensed phase simulation. *J. Chem. Phys.* **1987**, 86, 3462–3470.
- (10) Turi, L.; Borgis, D. Analytical investigations of an electron-water molecule pseudopotential. II. Development of a new pair potential and molecular dynamics simulations. J. Chem. Phys. 2002, 117, 6186–6195.
- (11) Jacobson, L. D.; Herbert, J. M. A oneelectron model for the aqueous electron that includes many-body electron-water polarization: Bulk equilibrium structure, vertical electron binding energy, and optical absorption spectrum. *J. Chem. Phys.* **2010**, 133, 154506.
- (12) Glover, W. J.; Schwartz, B. J. Short-range electron correlation stabilizes noncavity solvation of the hydrated electron. *J. Chem. Theory Comput.* **2016**, *12*, 5117–5131.
- (13) Marsalek, O.; Uhlig, F.; Vandevondele, J.; Jungwirth, P. Structure, dynamics, and reactivity of hydrated electrons by *ab initio* molecular dynamics. *Acc. Chem. Res.* **2012**, *45*, 23–32.
- (14) Savolainen, J.; Uhlig, F.; Ahmed, S.; Hamm, P.; Jungwirth, P. Direct observation of the collapse of the delocalized excess electron in water. *Nat. Chem.* **2014**, 6, 697–701.
- (15) Uhlig, F.; Herbert, J. M.; Coons, M. P.; Jungwirth, P. Optical spectroscopy of the bulk and interfacial hydrated electron from ab initio calculations. J. Phys. Chem. A 2014, 118, 7507-7515.

- (16) Kumar, A.; Walker, J. A.; Bartels, D. M.; Sevilla, M. D. A simple ab initio model for the hydrated electron that matches experiment. J. Phys. Chem. A 2015, 119, 9148– 9159.
- (17) Ambrosio, F.; Miceli, G.; Pasquarello, A. Electronic levels of excess electrons in liquid water. J. Phys. Chem. Lett. **2017**, 8, 2055–2059.
- (18) Wilhelm, J.; VandeVondele, J.; Rybkin, V. V. Dynamics of the bulk hydrated electron from many-body wavefunction theory. *Angew. Chemie Int. Ed.* **2019**, *58*, 3890–3893.
- (19) Holden, Z. C.; Rana, B.; Herbert, J. M. Analytic gradient for the QM/MM-Ewald method using charges derived from the electrostatic potential: Theory, implementation, and application to *ab initio* molecular dynamics simulation of the aqueous electron. *J. Chem. Phys.* **2019**, *150*, 144115.
- (20) Park, S. J.; Schwartz, B. J. Evaluating simple *ab initio* models of the hydrated electron: The role of dynamical fluctuations. *J. Phys. Chem. B* **2020**, *124*, 9592–9603.
- (21) Herbert, J. M.; Jacobson, L. D. Structure of the aqueous electron: Assessment of one-electron pseudopotential models in comparison to experimental data and time-dependent density functional theory. *J. Phys. Chem. A* **2011**, *115*, 14470–14483.
- (22) Luckhaus, D.; Yamamoto, Y.-I.; Suzuki, T.; Signorell, R. Genuine binding energy of the hydrated electron. *Sci. Adv.* **2017**, *3*, e1603224.
- (23) Nishitani, J.; ichi Yamamoto, Y.; West, C. W.; Karashima, S.; Suzuki, T. Binding energy of solvated electrons and retrieval of true UV photoelectron spectra of liquids. *Sci. Adv.* **2019**, *5*, 1–8.

- (24) Yamamoto, Y.-i.; Suzuki, T. Distortion Correction of Low-Energy Photoelectron Spectra of Liquids Using Spectroscopic Data for Solvated Electrons. *J. Phys. Chem. A* **2023**, *127*, 2440–2452.
- (25) Kevan, L. Electron spin echo studies of solvation structure. J. Phys. Chem. 1981, 85, 1628–1636.
- (26) Kevan, L. Solvated electron structure in glassy matrices. Acc. Chem. Res. 1981, 14, 138–145.
- (27) Coe, J. V.; Williams, S. M.; Bowen, K. H. Photoelectron spectra of hydrated electron clusters vs. cluster size: Connecting to bulk. *Intl. Rev. Phys. Chem.* **2008**, *27*, 27–51.
- (28) Coons, M. P.; Herbert, J. M. Quantum chemistry in arbitrary dielectric environments: Theory and implementation of nonequilibrium Poisson boundary conditions and application to compute vertical ionization energies at the air/water interface. J. Chem. Phys. 2018, 148, 222834.
- (29) Paul, S. K.; Coons, M. P.; Herbert, J. M. Erratum: "Quantum chemistry in arbitrary dielectric environments: Theory and implementation of nonequilibrium Poisson boundary conditions and application to compute vertical ionization energies at the air/water interface" [J. Chem. Phys. 148, 222834 (2018)]. J. Chem. Phys. 2019, 151, 189901.
- (30) Borsarelli, C. D.; Bertolotti, S. G.; Previtali, C. M. Thermodynamic changes associated with the formation of the hydrated electron after photoionization of inorganic anions: A time-resolved photoacoustic study. *Photochem. Photobiol. Sci.* **2003**, 2, 791–795.
- (31) Casey, J. R.; Schwartz, B. J.; Glover, W. J. Free energies of cavity and noncavity hydrated electrons near the instantaneous air/water interface. J. Phys. Chem. Lett. 2016, 7, 3192–3198.

- (32) Lockwood, D. M.; Rossky, P. J. Evaluation of functional group contributions to excess volumetric properties of solvated molecules. J. Phys. Chem. B 1999, 103, 1982–1990.
- (33) Marcus, Y. The standard partial molar volumes of ions in solution. Part 4. Ionic volumes in water at 0-100°C. J. Phys. Chem. B **2009**, 113, 10285–10291.
- (34) Herbert, J. M.; Coons, M. P. The hydrated electron. Annu. Rev. Phys. Chem. 2017, *68*, 447–472.
- (35) Lan, J.; Rybkin, V. V.; Pasquarello, A. Temperature dependent properties of the aqueous electron. Angew. Chem. Int. Ed. **2022**, e202209398.
- (36) Kirkwood, J. G.; Buff, F. P. The statistical mechanical theory of solutions. I. J. Chem. Phys. 1951, 19, 774–777.
- (37) Ben-Naim, A. The Kirkwood-Buff integrals for one-component liquids. J. Chem. Phys. 2008, 128, 234501.
- (38) Wu, Y.; Tepper, H. L.; Voth, G. A. Flexible simple point-charge water model with improved liquid-state properties. J. Chem. Phys. 2006, 124, 024503.
- (39) Krüger, P.; Schnell, S. K.; Bedeaux, D.; Kjelstrup, S.; Vlugt, T. J. H.; Simon, J.-M. Kirkwood–Buff integrals for finite volumes. J. Phys. Chem. Lett. 2013, 4, 235-238.
- (40) Krüger, P.; Vlugt, T. J. H. Size and shape dependence of finite-volume Kirkwood-Buff integrals. Phys. Rev. E 2018, 97, 051301.
- (41) Dawass, N.; Krüger, P.; Schnell, S. K.; Simon, J.-M.; Vlugt, T. J. H. Kirkwood-Buff integrals from molecular simulation. Fluid Ph. Equilibria 2019, 486, 21-36.

- (42) Primorac, T.; Požar, M.; Sokolić, F.; Zoranić, L. The influence of binary mixtures' structuring on the calculation of Kirkwood-Buff integrals: A molecular dynamics study. J. Mol. Lig. 2021, 324, 114773.
- (43) Bussi, G.; Donadio, D.; Parrinello, M. Canonical sampling through velocity rescaling. J. Chem. Phys. 2007, 126, 014101.
- (44) Bernetti, M.; Bussi, G. Pressure control using stochastic cell rescaling. J. Chem. Phys. 2020, 153, 114107.
- (45) Yang, C.-Y.; Wong, K. F.; Skaf, M. S.; Rossky, P. J. Instantaneous normal mode analysis of hydrated electron solvation dynamics. J. Chem. Phys. 2001, 114, 3598-3611.
- (46) Allen, M. P.; Tildesley, D. J. Computer simulation of liquids; Oxford university press, 2017.
- (47) Colbert, D. T.; Miller, W. H. A novel discrete variable representation for quantum mechanical reactive scattering via the S-matrix Kohn method. J. Chem. Phys. **1992**, 96, 1982–1991.
- (48) Shoemaker, D. P.; Garland, C. W.; Nibler, J. W. Experiments in Physical Chemistry; McGraw-Hill: New York, 1989.
- (49) Neupane, P.; Katiyar, A.; Bartels, D. M.; Thompson, W. H. Investigation of the Failure of Marcus Theory for Hydrated Electron Reactions. J. Phys. Chem. Lett. **2022**, 13, 8971–8977.
- (50) Toukan, K.; Rahman, A. Moleculardynamics study of atomic motions in water. Phys. Rev. B 1985, 31, 2643-2648.

# TOC Graphic

